Multiscale Finite Elements for Acoustics: Continuous, Discontinuous, and Stabilized Methods

I. Harari

Faculty of Engineering, Tel Aviv University, 69978 Ramat Aviv, Israel

ABSTRACT

This work describes two perspectives for understanding the numerical difficulties that arise in the solution of wave problems, and various advances in the development of efficient discretization schemes for acoustics. Standard, low-order, continuous Galerkin finite element methods are unable to cope with wave phenomena at short wave lengths because the computational effort required to resolve the waves and control numerical dispersion errors becomes prohibitive. The failure to adequately represent subgrid scales misses not only the fine-scale part of the solution, but often causes severe pollution of the solution on the resolved scale as well. Since computation naturally separates the scales of a problem according to the mesh size, multiscale considerations provide a useful framework for viewing these difficulties and developing methods to counter them. The Galerkin/least squares method arises in multiscale settings, and its stability parameter is defined by dispersion considerations. Bubble enriched methods employ auxiliary functions that are usually expressed in the form of infinite series. Dispersion analysis provides guidelines for the implementation of the series representation in practice. In the discontinuous enrichment method, the fine scales are spanned by free-space homogeneous solutions of the governing equations. These auxiliary functions may be discontinuous across element boundaries, and continuity is enforced weakly by Lagrange multipliers.

KEYWORDS

acoustics, Helmholtz equation, finite elements, stabilized methods, bubbles, discontinuous enrichment

*Address all correspondence to harari@eng.tau.ac.il, Phone +972-3-640-9439

1. INTRODUCTION

Wave problems present a major challenge to computation when the geometric length scale is large in proportion to the natural wavelength. This work describes two perspectives for understanding the numerical difficulties that arise in the solution of wave problems: loss of best approximation and failure to adequately represent subgrid scales. These views lead to various approaches to the development of efficient discretization schemes for acoustics, some of which are reviewed.

Computational acoustics has been an area of active research for almost half a century, also related to other fields of application such as geophysics, meteorology, electromagnetics, and so on. The challenge of efficient computation, at high wave numbers in particular, has been designated as one of the problems still unsolved by current numerical techniques [1]. Standard computational methods are unable to cope with wave phenomena at short wavelengths because they require a prohibitive computational effort to resolve the waves and control numerical dispersion errors. The failure to adequately represent subgrid scales misses not only the fine-scale part of the solution, but often causes severe pollution of the solution on the resolved scale as well. This phenomenon is related to the deterioration of numerical stability due to accumulation of dispersion errors. Many current discretization techniques are being developed in response to the challenge of controlling such errors effectively.

The Helmholtz equation describes time-harmonic acoustic and electromagnetic waves. The indefinite Helmholtz operator may lose ellipticity with increasing wave number since in that case, its weak form no longer induces a norm. This is related to the pollution effect, in which Galerkin finite element solutions with continuous low-order piecewise polynomials differ significantly from the best approximation [2] due to spurious dispersion in the computation, unless the mesh is sufficiently refined. In practical terms, pollution leads to a substantial increase in the cost of the finite element solution of the Helmholtz equation at higher wave numbers.

Domain-based methods such as finite elements are suitable for solving interior problems as well as exterior radiation and scattering problems in bounded domains that have been truncated by absorbing boundary conditions, infinite elements, or absorbing layers (see, e.g., the book by [3]). Historically, boundary element schemes based on integral equations [4–6], which do not require special treatment of the unbounded domain, were the preferred computational method in acoustics due to the reduced dimensionality of the domain, leading to fewer degrees of freedom. Over a decade ago, it became apparent that finite elements can be more efficient on large-scale problems because of the structure of their matrices in comparison to the global nature for boundary element discretization [7, 8]. While this conclusion becomes less obvious with the recent incorporation of fast multipole methods [9, 10], finite element methods retain the advantages of robustness and ease of integration with other discrete models in coupled problems.

2. ABSTRACT DIRICHLET PROBLEM

Let $\Omega \subset \mathbb{R}^d$ be a d-dimensional, open, bounded region with smooth boundary Γ.

For simplicity, consider the following (homogeneous) Dirichlet boundary value problem: find $u\colon \overline{\Omega} \to \mathbb{R}$ such that

$$\mathcal{L}u = f \qquad \text{in} \quad \Omega \tag{1}$$

$$u = 0 \qquad \text{on} \quad \Gamma \tag{2}$$

Here $f\colon \Omega \to \mathbb{R}$ is given. We think of $\mathcal{L}$ as a second-order differential operator. Generalization of the following results to problems with other types of boundary conditions and inhomogeneous boundary data, including radiation conditions representing unbounded domains, is straightforward. (See Sections 3.3, 4.3, and 5.3 for numerical results with other types of boundary conditions.)

The standard variational form is stated in terms of the set of functions $\mathcal{V} = H_0^1(\Omega)$: find $u \in \mathcal{V}$ such that

$$a(v,u) = (v,f), \qquad \forall v \in \mathcal{V} \tag{3}$$

Here $(\cdot,\cdot)$ is the $L_2(\Omega)$ inner product. (The form of the right-hand side assumes sufficiently smooth f.) The bilinear operator is related to the differential operator via integration by parts:

$$a(v,u) = (v,\mathcal{L}u) = (\mathcal{L}^*v,u) \tag{4}$$

for sufficiently smooth $u, v \in \mathcal{V}$.

The conventional finite element method is based on continuous Galerkin approximation in terms of the set of functions $\mathcal{V}^h \subset \mathcal{V}$, typically made up of continuous piecewise polynomials: find $u^h \in \mathcal{V}^h$ such that

$$a(v^h, u^h) = (v^h, f), \qquad \forall v^h \in \mathcal{V}^h \tag{5}$$

For some operators, this approach assures high coarse-mesh accuracy, but not for others.

2.1 Best Approximation: Nearly Optimal Petrov-Galerkin

The "best approximation" property can explain the difficulties that arise in some cases. When the bilinear operator is an inner product, the norm that it induces is often called the energy norm. Best approximation in the energy norm implies optimality of the finite element method in the sense that it minimizes the error $e = u^h - u$:

$$a(e, e) = a(U^h - u, U^h - u), \quad \forall U^h \in \mathcal{V}^h \tag{6}$$

For the Laplace operator the energy norm is the H^1 seminorm. In geometric terms, the finite element solution can be described as the H^1 projection of the unknown exact solution onto the finite-dimensional subspace

$$(\nabla v^h, \nabla u^h) = (\nabla v^h, \nabla u), \quad \forall v^h \in \mathcal{V}^h \tag{7}$$

This property is associated with nodal exactness in one dimension, but more importantly, it ensures good performance of multidimensional computation at any mesh resolution.

Best approximation in the energy norm is retained for many elliptic operators. Reaction-diffusion, where an undifferentiated term is added to the Laplace operator, is one such case. However, as the value of the reaction coefficient grows, the energy norm tends to the L_2 norm, losing the ability to control derivatives. The solution is still optimal, but in a norm that has become too weak. In computation, this takes the form of spurious oscillations in the vicinity of the thin layers that appear in the solutions of such problems, unless the mesh is sufficiently refined [11, 12].

In time-harmonic acoustics, governed by the Helmholtz equation, the sign of the undifferentiated term is reversed, and the coefficient is the wave number squared. As the wave number increases, the Helmholtz operator becomes indefinite and no longer induces a norm. This is related to the "pollution effect" [2], which can be interpreted physically as accumulation of spurious dispersion, or phase error.

Similar spurious phenomena related to the loss of good numerical performance at any mesh resolution by the standard finite element method are evident in other problems as well. In such cases, finite element computation can become prohibitively expensive in the presence of sharp gradients and rapid oscillations. This perspective motivates the development of methods that possess best approximation in the H^1 seminorm, as in Eq. (7), rather than the energy norm, retaining the high coarse-mesh accuracy of standard finite elements for the Laplace operator.

For simplicity, the following presentation is limited to operators for which the corresponding boundary operator is the normal derivative. Accounting for other cases merely requires additional notation. Partition the domain Ω in the usual way into n_{el} nonoverlapping regions Ω^e (element domains) with boundaries Γ^e, $e = 1, \ldots n_{\mathrm{el}}$. Denote the union of element interiors by

$$\widetilde{\Omega} = \bigcup_{e=1}^{n_{\mathrm{el}}} \Omega^e \tag{8}$$

Similarly, the union of element boundaries is denoted

$$\widetilde{\Gamma} = \bigcup_{e=1}^{n_{\mathrm{el}}} \Gamma^e \tag{9}$$

Following [13], assume that $\mathcal{V}^h$ is given. The solution of the Petrov-Galerkin equation

$$a(\bar{v}^h, u^h) = (\bar{v}^h, f), \quad \forall \bar{v}^h \in \bar{\mathcal{V}}^h \tag{10}$$

is optimal in the H^1 seminorm, as desired, provided that the weighting functions $\bar{v}^h \in \bar{\mathcal{V}}^h \subset \mathcal{V}$ satisfy

$$\mathcal{L}^* \bar{v}^h = -\Delta v^h \quad \text{in} \quad \widetilde{\Omega} \tag{11}$$

$$[\![\bar{v}^h_{,n}]\!] = [\![v^h_{,n}]\!] \quad \text{on} \quad \widetilde{\Gamma} \tag{12}$$

Here $[\![\cdot]\!]$ is the jump at an element boundary. Unfortunately, these functions are generally global and extremely difficult to find, except for some special cases [13, 14].

The goal, then, is to formulate a problem that retains optimality in the sense of Eq. (7), at least

approximately, yet may be solved readily. This is achieved by replacing the condition on the jump in normal derivatives across element boundaries (12) with the condition

$$\bar{v}^h = v^h \qquad \text{on} \quad \widetilde{\Gamma} \tag{13}$$

Note that the functions $v^{\mathrm{E}} = \bar{v}^h - v^h$ are bubbles over the elements, yet they are not residual-free, except in special cases such as piecewise linear Galerkin weighting functions on regular meshes.

The nearly optimal Petrov-Galerkin (NOPG) formulation [15] is stated in Eq. (10), with modified weighting functions defined in Eqs. (11) and (13). The label "nearly optimal" can be justified by the fact that this formulation approximates the H^1-optimal result (7), in the sense that its solution satisfies

$$(\nabla v^h, \nabla e) = (\llbracket v^h_{,n} - \bar{v}^h_{,n} \rrbracket, e)_{\widetilde{\Gamma}} \tag{14}$$

The nonzero right-hand side is a measure of the distance of the Petrov-Galerkin solution from H^1 optimality. This is related to the lack of symmetry of the formulation.

The basis for $\bar{\mathcal{V}}^h$ is defined on the element level, in terms of the standard local shape functions N_a. Since v^h in an element is expressed as a linear combination of nodal shape functions and arbitrary nodal coefficients, $\bar{v}^h$ is expressed as a similar linear combination of modified nodal shape functions $\bar{N}_a$ and the same arbitrary nodal coefficients. The modified shape functions are found by solving

$$\mathcal{L}^* \bar{N}_a = -\Delta N_a \qquad \text{in} \quad \Omega^e \tag{15}$$

$$\bar{N}_a = N_a \qquad \text{on} \quad \Gamma^e \tag{16}$$

The modified shape functions retain the interpolation property of the standard polynomial shape functions.

2.2 Variational Multiscale Framework

The multiscale perspective offers another interpretation of the lack of good numerical performance at any mesh resolution by the standard finite element method in some cases. Numerous approaches to alleviating this deficiency are based on modifications of the continuous piecewise polynomial Galerkin approximation. Several such related methods can be derived by the variational multiscale (VMS) approach [16, 17].

By this method, we consider an overlapping sum decomposition of the solution. In finite element computation, we have

$$\bar{u}^h = u^h + u^{\mathrm{E}} \tag{17}$$

Here $u^h \in \mathcal{V}^h$ is based on standard, finite element polynomials, representing coarse scales that are resolved by the mesh, and $u^{\mathrm{E}} \in \mathcal{V}^{\mathrm{E}}$ is an enhancement or enrichment, representing fine or subgrid scales, so that

$$\bar{\mathcal{V}}^h = \mathcal{V}^h \oplus \mathcal{V}^{\mathrm{E}} \tag{18}$$

Such a decomposition of the solution into a linear part and a bubble was already considered by [18]. The determination of the fine scales is key to the multiscale representation.

Following [17], we obtain a formula for the unresolved, fine scales

$$u^{\mathrm{E}} = M^{\mathrm{E}}(\mathcal{L}u^h - f) \tag{19}$$

in terms of the integral, generally nonlocal operator M^{E}, which depends on the space of fine scales (see [17] for details). The unresolved scales may be viewed as being driven by the residual of the resolved scales. This formula leads to an equation for the coarse scales:

$$\begin{aligned} a(v^h, u^h) + (\mathcal{L}^* v^h, M^{\mathrm{E}} \mathcal{L} u^h) &= (v^h, f) \\ + (\mathcal{L}^* v^h, M^{\mathrm{E}} f) & \end{aligned} \tag{20}$$

which includes the nonlocal effect of the fine scales. The term $\mathcal{L}^* v^h$ is interpreted as a Dirac distribution on the entire domain, with integrals over element interiors and jump terms integrated across element boundaries [17].

Various practical approximations arise from different treatments of the unresolved fine scales. The simplest approach is to employ a bubble representation of the fine scales [18–20], thereby localizing the effect of the fine scales. Solving a homogeneous Dirichlet, element-level problem for the fine scales is the approach that underlies the concept of residual-free bubbles (RFB) [21–23], as well as the related NOPG method. A similar result is obtained by employing an element Green's function [16], and the link to RFB was explored by [24]. The obvious limitation related to the loss of essential global effects inherent in local approaches may be overcome by employing nonconforming methods [25, 26]. The relationship of VMS methods based on *fine-scale* Green's

functions to optimal stabilized methods with global and local character is described by [27].

3. LEAST SQUARES STABILIZATION

Some stabilized methods may be derived directly within the VMS framework as well, and others are closely related. Stabilized methods stand out among the numerous improved approaches by combining substantial improvement in performance with extremely simple implementation.

3.1 Methods

Stabilized methods of adjoint type

$$\begin{aligned} a(v^h,u^h)\ &-(\mathcal{L}^*v^h,\tau\mathcal{L}u^h)_{\tilde{\Omega}}=(v^h,f)\\ &-(\mathcal{L}^*v^h,\tau f)_{\tilde{\Omega}} \end{aligned} \tag{21}$$

also called "unusual stabilized finite element methods" [28, 29], may be derived in the VMS framework and are related to RFB. The additional stabilizing terms (cf. Eq. (5)), are integrated over element interiors to respect regularity requirements of typical, piecewise smooth, finite element functions, superseding the distributional interpretation in this case. In practice, standard finite element procedures that assemble global arrays from element contributions are employed without modification. The stability parameter τ is defined on the element level, depending on the element size, the finite element interpolation, and the coefficients of the problem. The structure of the additional stabilizing terms compared to Eq. (20) indicates that the stability parameter provides an algebraic approximation of the integral operator M^{E}.

In practice, for the self-adjoint Helmholtz operator, this method is form-identical to the Galerkin/least squares (GLS) method [12]

$$a(v^h,u^h)+(\mathcal{L}v^h,\tau\mathcal{L}u^h)_{\tilde{\Omega}}=(v^h,f)+(\mathcal{L}v^h,\tau f)_{\tilde{\Omega}} \tag{22}$$

(the only difference is in the sign of the stability parameter). The stability parameter for acoustics is usually defined by dispersion considerations [12, 30, 31], which typically don't account for unstructured meshes, although improved performance in computation is not limited to structured meshes [30, 32]. There is recent progress in the definition of the stability parameter for distorted elements [33]. The VMS distributional interpretation motivated the development of a stabilized method that includes the inter element jump terms [34], which are usually omitted in the local approach.

The related method of Galerkin-gradient/least squares (GGLS),

$$\begin{aligned} a(v^h,u^h)\ &+(\nabla\mathcal{L}v^h,\tau^{\mathrm{G}}\nabla\mathcal{L}u^h)_{\tilde{\Omega}}=(v^h,f)\\ &+(\nabla\mathcal{L}v^h,\tau^{\mathrm{G}}\nabla f)_{\tilde{\Omega}} \end{aligned} \tag{23}$$

was originally developed to stabilize problems governed by the modified Helmholtz equation [12], and was later shown to be effective on the Helmholtz equation as well [35]. The GLS and GGLS methods are quite similar for linear finite elements. In fact, both produce *identical* solutions on structured meshes of linear elements (for constant-coefficient Dirichlet problems with uniform source distributions, see [35]). Numerical comparisons of the two methods in more elaborate configurations show that their performance is similar [30].

3.2 Stability Parameter by Dispersion Analysis

Consider time-harmonic acoustics, where $\mathcal{L}u = -\Delta u - k^2u$ is the self-adjoint, indefinite, Helmholtz operator with given wave number k. Dispersion analysis of numerical methods for the Helmholtz equation examines the dependence of the numerical error on mesh resolution as well as mesh orientation, by comparison to exact, free-space solutions of the constant-coefficient, homogeneous equation, typically in the form of plane waves. These ideas can be extended to cylindrical and spherical waves as well [36]. The analysis measures the performance of the standard Galerkin method and provides a tool for the design of improved methods. A homogeneous, isotropic continuum is nondispersive. This is usually no longer the case for discrete representations. Each numerical method is characterized by a resolution-dependent approximate wave number, which accounts for numerical dispersion.

Free-space solutions of the homogeneous Helmholtz equation with constant wave number are plane waves:

$$u=\exp(\mathrm{i}\mathbf{k}\cdot\mathbf{x}) \tag{24}$$

Here $|\mathbf{k}|=k$. For a plane wave propagating in the θ direction in two dimensions, $\mathbf{k}^T=k\langle c,s\rangle$, $c=\cos\theta$, and $s=\sin\theta$.

In contrast to exact solutions in isotropic continua, numerical solutions are anisotropic in the sense that they depend on the orientation of the mesh with respect to the direction of propagation, in addition to mesh resolution. This phenomenon is known for both Cartesian [31, 34, 37–44] and triangular [40, 43] mesh topologies.

The finite element representation of a plane wave parallel to element faces on a uniform three-dimensional mesh of hexahedra is identical to propagation at an arbitrary direction in two dimensions. Consider a uniform two-dimensional mesh of four-noded bilinear quadrilateral elements of size h, aligned with the global axes, with nodal points located at (mh, nh), $m, n \in \mathbb{Z}$. Values of a plane wave in two dimensions (24), oriented at an angle θ to the mesh, at the nodal points are

$$u(mh, nh) = (\exp(\mathrm{i}khc))^m (\exp(\mathrm{i}khs))^n \qquad (25)$$

Dispersion analysis considers corresponding nodal values of finite element solutions in the form

$$u^h(mh, nh) = (\exp(\mathrm{i}k^h hc))^m (\exp(\mathrm{i}k^h hs))^n \qquad (26)$$

The following analysis determines the dependence of the approximate wave number k^h on the mesh resolution

$$G = \frac{2\pi}{kh} \qquad (27)$$

(representing the number of nodal points per wavelength) and orientation. Each internal node in a structured planar mesh of bilinear quadrilaterals is shared by four elements. In the banded global coefficient matrix, the equation for each internal node depends only on the values of the nodes belonging to those four elements—nine nodes altogether. Consequently, the dispersion analysis considers such a typical nine-point patch (Fig. 1).

Substituting the plane wave form (26) into the nine-point stencil that arises at any interior node yields the following Galerkin dispersion relation for a Cartesian mesh aligned with element faces parallel to a plane wave:

$$\begin{aligned}(kh)^2 = 6\Big(&4 - \cos(k^h hc) - \cos(k^h hs) \\ &-2\cos(k^h hc)\cos(k^h hs)\Big)\Big/\Big((2+\cos(k^h hc)) \\ &\times(2 + \cos(k^h hs))\Big)\end{aligned} \qquad (28)$$

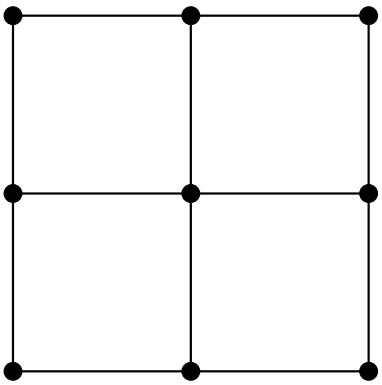

FIGURE 1. Nine-node Cartesian patch

The variation with respect to the direction of propagation θ is a manifestation of anisotropy.

This is an implicit relation for k^h. The response is a symmetric function of orientation, with a periodicity of $\pi/2$. Consequently, it is sufficient to examine the response between 0 and $\pi/4$. Values of $k^h h$ satisfying the implicit relation (28) for intermediate orientations are obtained numerically, and are shown in Fig. 2, for different levels of the mesh resolution (see Eq. (27)). Note that the bilinear element solution is *more* dispersive when the mesh is aligned *with* waves. The dispersion varies approximately 50% with the orientation.

The stability parameter of stabilized methods is usually defined by dispersion considerations. The original form of the GLS method for acoustics [12]

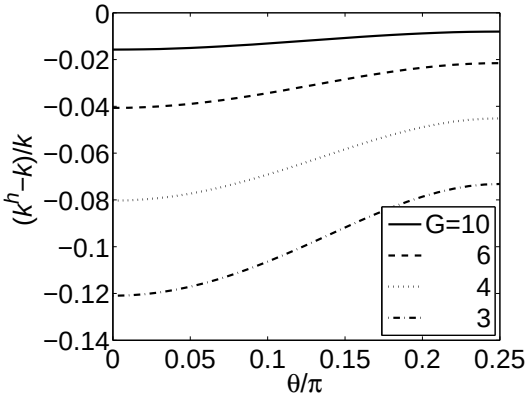

FIGURE 2. Dispersion of the bilinear element at various resolutions, $G = 2\pi/(kh)$

incorporates a stability parameter that eliminates dispersion on uniform meshes of quadrilaterals aligned with the direction of propagation ($Q-0$):

$$\tau k^2 = 1 - \frac{6}{(kh)^2}\,\frac{1-\cos(kh)}{(2+\cos(kh)} \tag{29}$$

This was generalized to other directions of propagation [31] such as eliminating dispersion when element diagonals are aligned with the direction of propagation ($Q-\pi/4$). In particular, the bisecting direction ($Q-\pi/8$) was advocated. Extending these ideas to linear triangular elements, the parameter is defined by dispersion on hexagonal patches, which exhibit low anisotropy [45]. The method parameter that eliminates spurious dispersion of plane waves along the altitude of linear triangular elements in a hexagonal mesh topology ($T-\pi/6$) is quite simple,

$$\tau k^2 = 1 - \frac{8}{(kh)^2}\,\frac{1-\cos(\sqrt{3}kh/2)}{(2+\cos(\sqrt{3}kh/2)} \tag{30}$$

yet provides an excellent approximation of the parameter Q-$\pi/8$. Figure 3 compares the stability parameters.

The definition of the element size h is a matter of consequence in computational methods with mesh-dependent parameters. The stability parameters are usually defined from dispersion analyses, which are performed on uniform meshes. The natural definition of the mesh size is the element side in such cases. However, the generalization of this concept to unstructured meshes is less clear-cut. Possible options for quadrilaterals are the average element side (i.e., a quarter of the perimeter), the square root of the area, and the ratio of the area to the average element side. These alternatives coincide with the usual definition on uniform meshes.

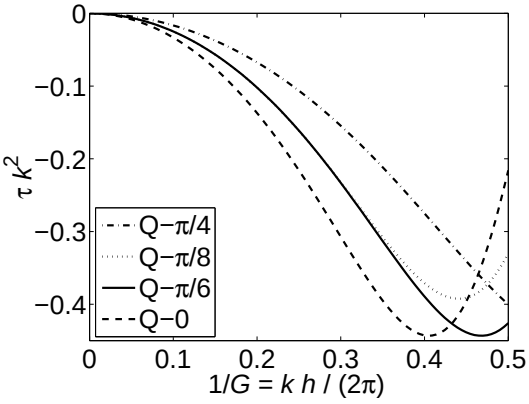

FIGURE 3. GLS stability parameters

3.3 Numerical Results

A series of computations compares the numerical performance of the GLS and GGLS methods for several configurations with different kinds of boundary conditions employing structured and unstructured meshes of four-noded quadrilaterals [30]. The numerical tests examine the effects of different definitions of the stability parameters as well as definitions of the element size on which they depend. Results for radiation in an automotive interior are reported as a sample of these numerical tests.

Consider a domain related to a car compartment (Fig. 4) with no distributed sources ($f=0$), similar to a problem solved by [46, 47]. Of the two wave numbers examined, $kL=5$ and 20 (nondimensionalized by the length of the compartment), only results for the higher wave number with relatively low resolution are reported. The boundary conditions, representing acoustic properties of a simplified car construction, are a plane wave in the direction $\theta=\pi/3.6$ for the vibration of the firewall, an impedance condition with $\alpha=0.9$ for the absorbing roof and a homogeneous Neumann condition elsewhere. The domain is discretized by a set of three increasingly refined unstructured meshes (Fig. 5). In the coarsest mesh, there are 127 nodes with 100 quadrilaterals. The resolution in this mesh ranges from 3.56 to 29.1 (with a mean over the resolutions of 6.54) points per wavelength. The lower limit of resolution in this mesh is clearly insufficient to resolve the higher wave number adequately.

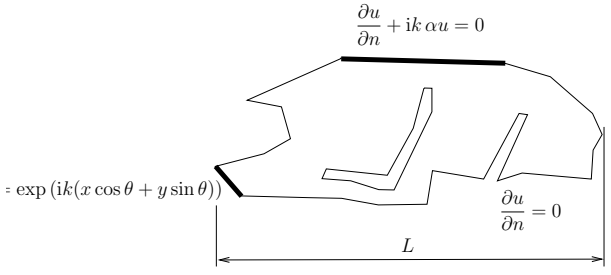

FIGURE 4. Radiation in an automotive interior: domain and boundary conditions

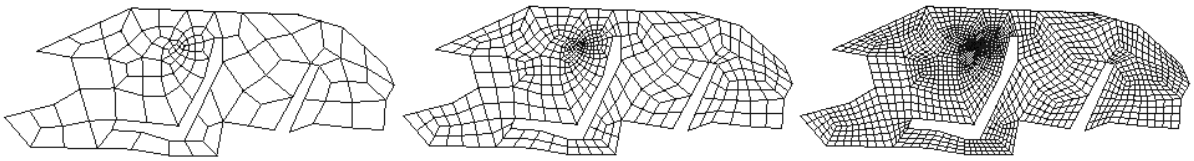

FIGURE 5. Radiation in an automotive interior: meshes

In the intermediate mesh, there are 454 nodes with 400 quadrilaterals. The resolution in this mesh ranges from 6.93 to 60.7 (with a mean of 13.2) points per wavelength. In the finest mesh, there are 1708 nodes with 1600 quadrilaterals. The resolution in this mesh ranges from 13.7 to 124 (with a mean of 26.6) points per wavelength.

A Galerkin reference solution is computed with a mean resolution of 212 points per wavelength. The differences between the various methods are negligible at this high resolution. Results obtained with various definitions of the stability parameter, and the element size h defined as the average side of an element (or one-quarter of the perimeter), are reported in Fig. 6. The stabilized methods exhibit superior performance on these unstructured meshes. In fact, at the lowest resolution, the Galerkin results are not physically meaningful, yet the stabilized methods consistently provide reasonable solutions even at very low resolutions (recall that the

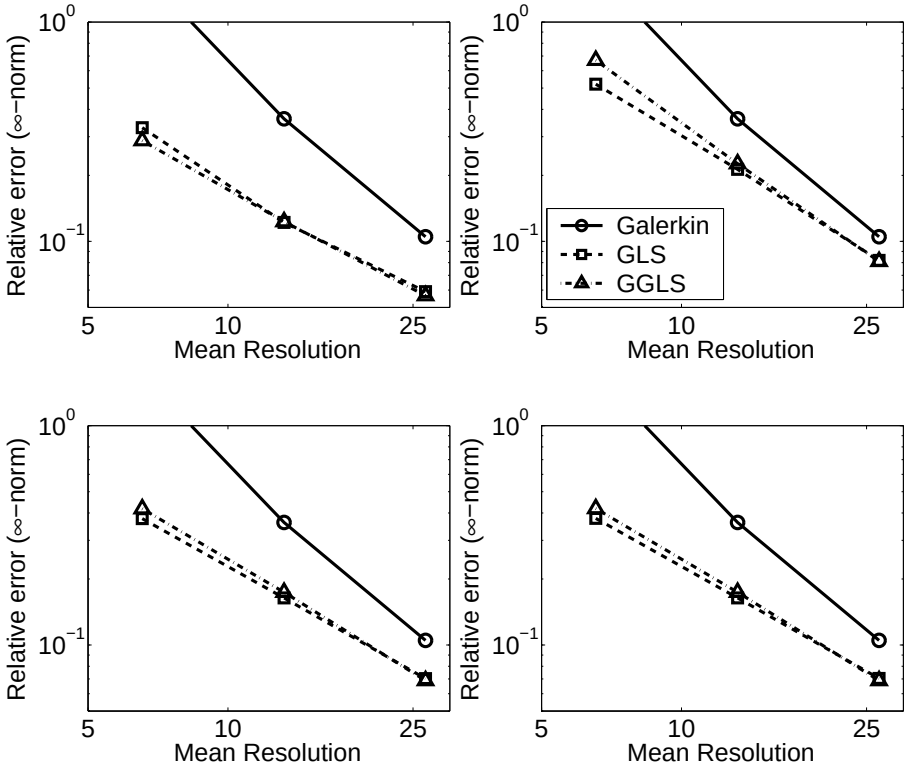

FIGURE 6. Radiation in an automotive interior: $kL = 20$ and element size defined as the average side; $Q - 0$ (top, left), $Q - \pi/4$ (top, right), $Q - \pi/8$ (bottom, left), and $T - \pi/6$ stability parameters. (The mean resolution is the average over resolutions of the unstructured meshes)

lowest resolution on the coarsest mesh is 3.56 points per wavelength). The GLS method usually provides better results on coarser meshes. A comparison of the stability parameters repeats the pattern observed previously: that the results of the $Q-0$ parameter are uniformly the best, whereas those of the $Q-\pi/4$ parameter are invariably the worst. Results of the $Q-\pi/8$ and the simpler $T-\pi/6$ parameters, virtually indistinguishable from each other even at these lower resolutions, lie between these two extremes.

4. BUBBLE STABILIZATION

The RFB and NOPG improved methods, obtained by bubble-based enrichment, are closely related, and identical in some cases.

4.1 Methods

The NOPG formulation [15] is stated in Eq. (10), with modified weighting functions defined in Eqs. (11) and (13).

To define the RFB method, we assume that $\mathcal{V}^h$ is given and that the enrichment functions u^{E} (and v^{E}) are element-level bubbles; that is, they vanish at element interfaces. The fine-scale problem can then be written in strong form:

$$\mathcal{L}u^{\mathrm{E}} = -(\mathcal{L}u^h - f) \qquad \text{in} \qquad \widetilde{\Omega} \tag{31}$$

$$u^{\mathrm{E}} = 0 \qquad \text{on} \qquad \widetilde{\Gamma} \tag{32}$$

In this case, the coarse-scale equation is simplified since the interelement jumps in the second term on the left-hand side vanish due to the bubble nature of the enrichment functions, leaving only integrals over element interiors:

$$a(v^h, u^h) + (\mathcal{L}^* v^h, u^{\mathrm{E}})_{\widetilde{\Omega}} = (v^h, f) \tag{33}$$

This is the RFB problem, with the residual-free bubbles defined in Eqs. (31) and (32).

Remark. This form of the equation justifies the use of simplifications of u^{E} in practical implementation. For advection-diffusion, a reduced solution for the advective limit is considered, lacking a thin boundary layer along the outflow boundary to satisfy compatibility requirements. The presence of such a boundary layer is of little consequence in the integration of the bubble in Eq. (33) so that it may be replaced in practice by the simpler reduced solution with interelement jumps.

The basis for $\mathcal{V}^{\mathrm{E}}$ is defined on the element level, in terms of N_a, the standard polynomial shape function of local node a. Since u^h in an element is expressed as a linear combination of nodal polynomial shape functions and nodal coefficients, u^{E} is also expressed as a linear combination of nodal bubble basis functions b_a and the same nodal coefficients. The bubble basis functions are found by solving

$$\mathcal{L}b_a = -(\mathcal{L}N_a - f) \qquad \text{in} \quad \Omega^e \tag{34}$$

$$b_a = 0 \qquad \text{on} \quad \Gamma^e \tag{35}$$

To compare the two methods, recall that the RFB method can be written in terms of a modified approximate solution

$$\bar{u}^h = u^h + u^{\mathrm{E}} \tag{36}$$

and the the modified weighting function of NOPG can be expressed in terms of a bubble

$$\bar{v}^h = v^h + v^{\mathrm{E}} \tag{37}$$

In both cases, the nodal basis can be formed either in terms of modified shape functions or bubble basis functions

$$\bar{N}_a = N_a + b_a \tag{38}$$

Thus the modified shape function can be defined directly or via the bubble basis function.

The element-level auxiliary boundary value problem that defines the RFB bubble basis functions can also be stated in terms of modified shape functions, and conversely the NOPG problem for modified shape functions can also be expressed for bubble basis functions [48]. The boundary conditions for both methods, either in terms of modified shape functions or bubble basis functions, are identical, and the governing differential equations are quite similar.

The differential operators are identical for the self-adjoint Helmholtz operator. The differences between the auxiliary functions of the two methods lie in the presence of the given function f and the Laplacian of the standard shape function ΔN_a. The performance of numerical methods for problems of acoustics is often evaluated by dispersion analysis, which examines homogeneous solutions on regular meshes. Under these conditions, again, the functions for the two methods are identical.

Remark. In many cases, the two methods with identical auxiliary functions lead to the same nodal solutions. However, the RFB solution is enriched with bubbles, whereas the NOPG solution is not. Thus the RFB method may exhibit superior performance measured in an integral norm (see Section 4.3).

In summary, the auxiliary functions are expressed either by modified shape functions that satisfy a homogeneous Helmholtz equation within the element with inhomogeneous Dirichlet boundary conditions on the element boundary,

$$\mathcal{L}\bar{N}_a = 0 \quad \text{in} \quad \Omega^e \tag{39}$$

$$\bar{N}_a = N_a \quad \text{on} \quad \Gamma^e \tag{40}$$

or by bubble basis functions that satisfy an inhomogeneous Helmholtz equation within the element with homogeneous Dirichlet boundary conditions on the element boundary,

$$\mathcal{L}b_a = k^2 N_a \quad \text{in} \quad \Omega^e \tag{41}$$

$$b_a = 0 \quad \text{on} \quad \Gamma^e \tag{42}$$

4.2 Auxiliary Functions

Several expressions for the auxiliary functions were derived independently, without recognizing the connection between them. Beginning with a two-noded linear element of length h in one dimension, $a = 1$ or 2, the parent domain is the biunit interval with nodal coordinate $\xi_a = (-1)^a$. The linear shape functions are

$$N_a = \frac{1}{2}(1 + \xi_a \xi), \qquad a = 1, 2 \tag{43}$$

The modified shape functions [15]

$$\bar{N}_a = \frac{\sin\left(khN_a(\xi)\right)}{\sin kh} \tag{44}$$

are expressed concisely in terms of the linear shape functions, satisfying the element-level boundary value problems (39) and (40). As expected, $\bar{N}_a \to N_a$ as $kh \to 0$. The modified shape functions become unbounded at $kh = \pi$, the first resonance of the boundary value problems (39) and (40). This corresponds to an unrealistically low mesh resolution of $G = 2$ and thus poses no practical difficulty.

As a prelude to the more complicated two-dimensional configurations, consider an alternative representation for the one-dimensional case as an infinite series for the bubbles. The bubble basis function is expressed in terms of eigenfunctions of the Dirichlet problem for the Laplacian

$$b_a = \sum_{n=1}^{\infty} A_n \sin\left(n\pi N_a(\xi)\right) \tag{45}$$

satisfying the homogeneous boundary conditions (42). To satisfy the inhomogeneous differential Eq. (41), by orthogonality,

$$A_n = \frac{2}{n\pi} \frac{(-1)^n}{1 - \left(\frac{n\pi}{kh}\right)^2} \tag{46}$$

At resolutions over $G = 2$ (i.e., $kh < \pi$), the boundary value problems (39)–(40) and (41)–(42) have unique solutions so that the modified shape functions (44) and the full series representation of the bubble basis functions (45) satisfy the relationship (38).

Consider a four-noded bilinear square element of side h in two dimensions. Three series representations are outlined for this case, with more details provided by [48]. The first is a simplification of a double-index series derived in a manner similar to that just presented in one dimension [15], denoted here BH. The bubble basis function is again expressed in terms of eigenfunctions of the Dirichlet problem for the Laplacian, satisfying the homogeneous boundary conditions (42), with coefficients determined by orthogonality to satisfy the inhomogeneous differential Eq. (41). In practice, the series is truncated after a finite number of terms. Let M and N denote the upper limit of each index. We consider only cases in which $M = N$.

An alternative approach was employed in the first application of the RFB method to the Helmholtz equation [22], denoted here FFML. Separation of variables leads to a single-index series for the modified shape function, satisfying the homogeneous Eq. (39), with coefficients determined by orthogonality to satisfy the inhomogeneous boundary conditions (40). In practice, the series is truncated after M terms. Numerical tests were performed with $M = 200$ terms in this series [22, 40].

An unpublished approach (C. Farhat personal communication, 1996), denoted here CF, also considers the bubble. A single-index series is obtained

by separation of variables, treating the homogeneous and particular solutions in one of the directions separately and satisfying the homogeneous boundary conditions (42), with coefficients that ensure satisfaction of the inhomogeneous Eq. (41). Again, in practice, the series is truncated after M terms.

As in the one-dimensional case, the boundary value problems (39)–(40) and (41)–(42) have unique solutions at resolutions over $G = 2$ (i.e., $kh < \pi$). Thus the *full* series representations of the BH and CF bubble basis functions are equal and, together with the FFML modified shape functions, satisfy the relationship (38). As a practical guideline, we wish to determine which of these three alternative series, BH, FFML, or CF, provides adequate representation of the improved shape functions with the fewest terms, and the number of terms that should be used.

In the practical implementation of the bubble-enriched methods, dispersion depends on the number of terms employed in the series M. Let k_M^h denote the approximate wave number obtained by the truncated representation of a given series. The approximate wave number k^h is obtained by the full representation of any of the series (computed by taking a large number of terms in one of the series). The incremental error in the approximate wave number,

$$e = \frac{k_M^h - k_{M-1}^h}{k_{M-1}^h} \tag{47}$$

is used to evaluate the convergence of each series. The incremental error for each series depends also on the resolution and orientation. The dependence of the incremental error on the number of terms in two of the series, for a low resolution of $G = 4$ and an intermediate resolution of $G = 10$, and the two extreme values of orientation, are shown in Fig. 7.

The number of terms in each series required to keep the incremental error in the approximate wave number below a threshold of 10^{-4} is shown in Table 1. The CF series with six terms provides this accuracy at any resolution above four points per wavelength. Consequently, we advocate the use of the CF series with about six terms for the four-noded RFB and NOPG elements.

Now that the bubble representation has been determined, the dispersion properties of the four-noded RFB and NOPG elements can be examined.

TABLE 1. The number of terms required in each series to bound the incremental error in the approximate wave number by $e < 10^{-4}$, see Fig. 7

G	BH	FFML	CF
10	4×4	18	4
4	6×6	16	6

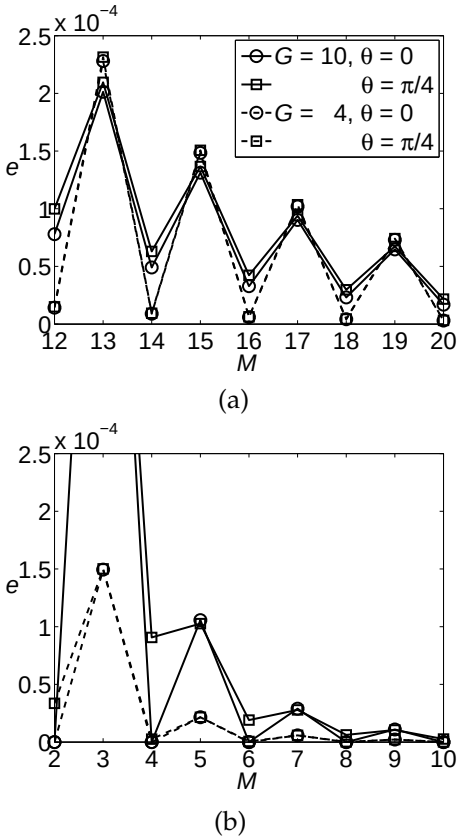

FIGURE 7. Incremental error in the approximate wave number $e = k_M^h/k_{M-1}^h - 1$ of the truncated FFML **(a)**, and CF series **(b)**

Of course, all three series representations converge to the same dispersion behavior with a sufficient number of terms. Figure 8 (left) shows the dependence of the relative error in wave number on the orientation of the mesh with respect to the direction of propagation, varying between the two extreme cases of propagation. The reduction in dispersion of the bubble-enriched methods over the standard Galerkin method is clear, most noticeably at the lower resolutions. The particularly good per-

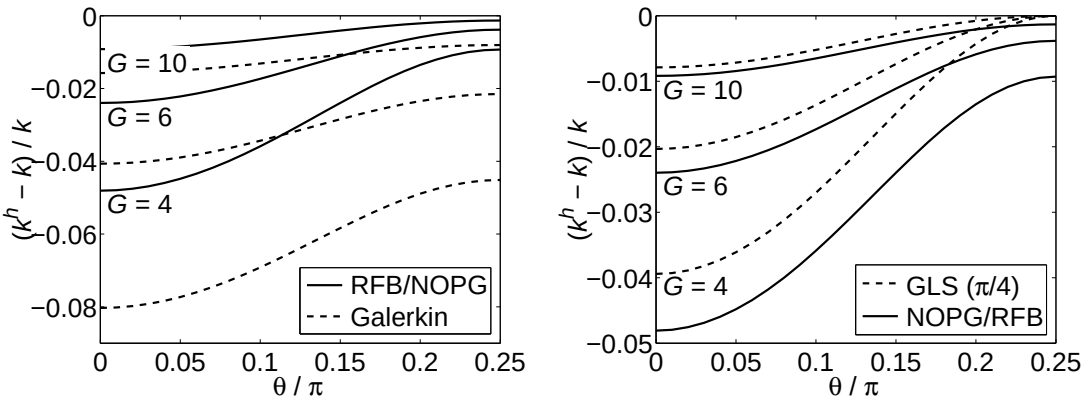

FIGURE 8. Dispersion error of four-noded elements: bubble-enriched vs. Galerkin (left), and vs. GLS $Q - \pi/4$

formance of the improved methods along element diagonals is striking and agrees with behavior observed in numerical tests for advection-diffusion [21].

The superior performance of the bubble-enriched methods over the Galerkin method motivates the comparison to other improved methods such as the GLS-stabilized method. Figure 8 (right) compares the behavior of the bubble-enriched methods to that of the version of GLS that eliminates spurious dispersion along element diagonals ($Q - \pi/4$). In this case, the dispersion properties of GLS are superior at every resolution.

4.3 Numerical Results

A series of computations examines the numerical performance of the bubble-enriched methods, employing structured and unstructured meshes of four-noded quadrilaterals for several wave guide problems. The bubble enrichment is based on the CF representation with six terms, as recommended by the dispersion analysis. The behavior is compared to the version of the least squares stabilized method that eliminates spurious dispersion of plane waves in the bisecting direction, as advocated by [31], and denoted GLS ($\pi/8$). Results of some of these numerical tests are reported.

Consider an $a \times a$ square with $ka = 8$ and no distributed sources ($f = 0$). Two cases are considered, defined by different combinations of boundary conditions (to be specified subsequently) that are imposed on the boundaries of the square so that the exact solution is a plane wave propagating in a given direction (24).

The domain is discretized by two sets of three increasingly refined meshes each. The first set consists of nested uniform meshes of 8×8, 16×16, and 32×32 elements, that is, the element sides are halved from one level of refinement to the next (Fig. 9). The cor-

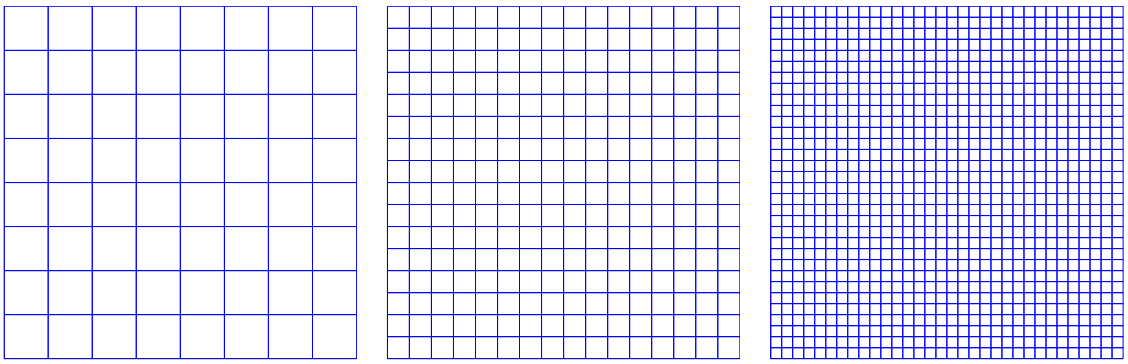

FIGURE 9. Uniform meshes

responding resolutions are 6.3, 12.6, and 25.1 points per wavelength.

The other set consists of three nonuniform meshes each (Fig. 10). These meshes contain highly distorted elements with large variations in mesh size to test computational performance under extreme conditions. Each mesh has a mean element size roughly the same as the corresponding uniform mesh. The element size of a distorted element is taken as the average side of the element. The bubble enrichment is originally constructed for square elements. The same functions, defined in the parent domain, are used for general quadrilateral elements as well, although they don't satisfy the auxiliary boundary value problems exactly in distorted elements. Integration in distorted elements is performed with 2×2 Gaussian quadrature.

The first case presented is a plane wave aligned with the x-axis, that is, $\theta = 0$ in Eq. (24), specified by appropriate inhomogeneous Dirichlet boundary conditions on the boundaries that are normal to the x-axis and homogeneous Neumann boundary conditions on the boundaries that are normal to the y-axis. Results for the various meshes are reported in Fig. 11, measured in the H^1 seminorm. Nodal results of the NOPG and RFB methods on meshes that are not uniform are indistinguishable, although not theoretically identical. Accounting for the bubble enrichment in the RFB results (i.e., interpolating the nodal results by the modified shape functions that include polynomials and bubbles), denoted RFB(+), considerably reduces the error. The RFB/NOPG results are comparable to GLS ($\pi/8$) and slightly better than the Galerkin solution, particularly at lower resolutions. However, the RFB(+) results are noticeably superior.

Inhomogeneous Robin boundary conditions are now specified on all boundaries so that the exact so-

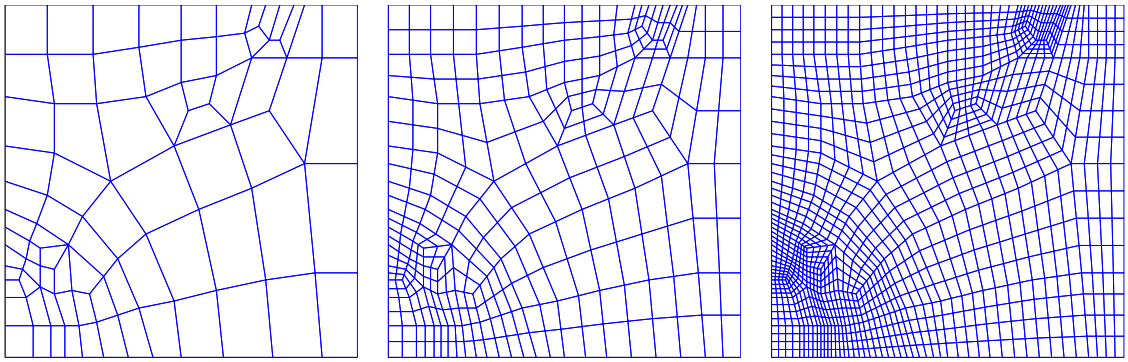

FIGURE 10. Unstructured meshes

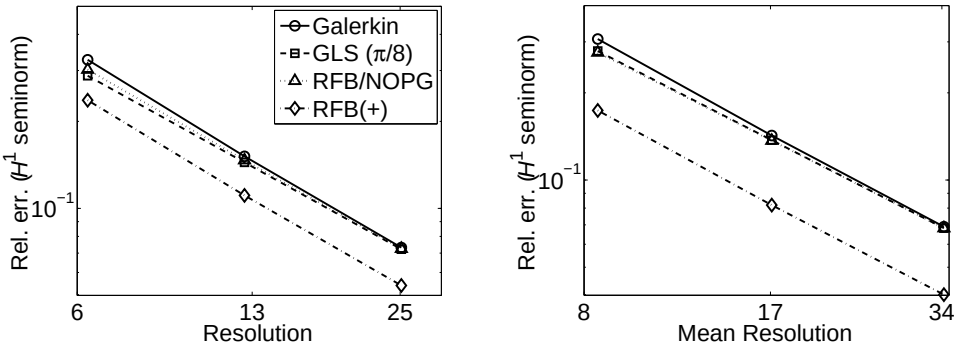

FIGURE 11. Wave guide at $\theta = 0$, Dirichlet-Neumann boundary conditions: structured (left) and unstructured meshes

lution is a plane wave propagation at an angle of $\theta = \pi/4$ with respect to the x-axis (see Eq. (24)). Results for the various meshes are reported in Fig. 12. The performance observed in the previous case is repeated here, namely, that the RFB/NOPG results are comparable to GLS ($\pi/8$) and slightly better than the Galerkin solution, particularly at lower resolutions, and the RFB(+) results are noticeably superior.

5. DISCONTINUOUS ENRICHMENT METHOD

An alternative approach that has appeared predominantly in time-harmonic acoustic applications is to base the fine scales on free-space solutions of the homogeneous differential equation (e.g., plane waves in the case of the Helmholtz equation). These functions are often readily available, but are typically global, and hence require specialized treatment in practice. The generalized finite element method (GFEM) of [49] is an extension of the partition of unity method (PUM) of [50], applied to acoustics [51], in which the free-space homogeneous solutions are multiplied by conventional finite element shape functions. The piecewise polynomial shape functions localize the free-space homogeneous solutions and provide interelement continuity. In PUM, the product of free-space homogeneous solutions and finite element shape functions constitutes the entire approximation, whereas in GFEM, only the fine scales are based on this product, together with conventional finite element functions for the coarse scales, thus alleviating the severe ill-conditioning to which PUM is susceptible. The efficient integration of oscillatory functions is also a crucial issue in these methods.

Similar ideas for incorporating features of the differential equation in the approximation, but in discontinuous frameworks with specialized treatment for interelement continuity, go back to the weak element method [52], as well as the recent ultra weak variational formulation [53] and least squares method [54]. Similarly, the variational theory of complex rays is based on a formulation in which admissible solutions satisfy the differential equation, and interelement continuity is enforced weakly by average flux-type quantities. This method was developed for structural vibrations [55], and its extension to acoustics should be straightforward. Such formulations closely resemble Trefftz approaches (see, e.g., [56]). As in PUM, the special basis functions in these methods *replace* the standard finite element polynomials. Various implementations of hybrid approaches combining finite elements with wave-based methods have been suggested [57, 58]. Some discontinuous formulations employ finite element polynomials, instead of oscillatory basis functions [59].

5.1 Fine Scales

In the discontinuous enrichment method (DEM), standard finite element polynomials are retained for the coarse scales and are enriched within each element by nonconforming free-space homogeneous solutions representing fine scales, with continuity enforced in the variational formulation [60]. This approach, applicable to general multiscale computation [61], is also applied to elastic wave [62] and fluid structure analysis [63, 64].

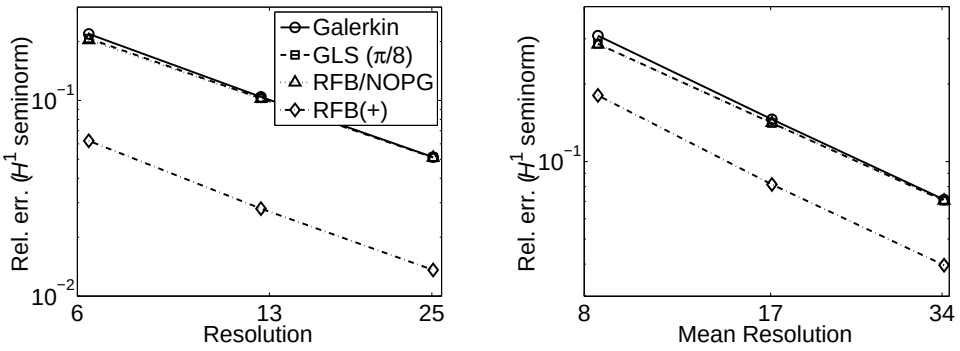

FIGURE 12. Wave guide at $\theta = \pi/4$, Robin boundary conditions: structured (left) and unstructured meshes

The strategy that underlies DEM is based on the assumption that particular solutions are usually well resolved and thus may be considered coarse scales. The fine scales should therefore contain solutions of the homogeneous partial differential equation. This interpretation of the fine scales differs somewhat from that of conventional multiscale numerical representations. Weak enforcement of interelement continuity permits the use of free-space solutions, that is, $\mathcal{V}^{\mathrm{E}}$ is spanned by solutions of

$$\mathcal{L}u^{\mathrm{E}} = 0 \qquad \text{in} \quad \mathbb{R}^d \tag{48}$$

that are not already represented in the polynomial basis, leading to relative ease of implementation, yet retaining global, fine-scale effects.

The discontinuous Galerkin approximation is stated in terms of the set of functions $\mathcal{V}^h \subset L_2(\Omega) \cap H^1\left(\widetilde{\Omega}\right)$, with Lagrange multiplier approximations $\lambda^h \in \mathcal{W}^h \subset H^{-1/2}\left(\widetilde{\Gamma}\right)$ defined on the union of element interiors $\widetilde{\Gamma}$ (and corresponding weights μ^h). The hybrid variational formulation that underlies DEM may be decomposed as

$$a(v^h, u^h) + a(v^h, u^{\mathrm{E}}) - \langle \lambda^h, v^h \rangle \;\; = (v^h, f) \tag{49}$$

$$a(v^{\mathrm{E}}, u^{\mathrm{E}}) + a(v^{\mathrm{E}}, u^{\mathrm{E}}) - \langle \lambda^h, v^{\mathrm{E}} \rangle_{\widetilde{\Gamma}} = (v^{\mathrm{E}}, f) \tag{50}$$

$$-\langle \mu^h, u^h \rangle - \langle \mu^h, u^{\mathrm{E}} \rangle_{\widetilde{\Gamma}} - \langle \lambda^h, v^{\mathrm{E}} \rangle_{\widetilde{\Gamma}} = 0 \tag{51}$$

Here $\langle \cdot, \cdot \rangle$ is the duality pairing between $H^{-1/2}(\Gamma)$ and $H^{1/2}(\Gamma)$. Allowing for discontinuities, the weak operator in this case is $a(v, p) = (\nabla v, \nabla p)_{\widetilde{\Omega}} - (v, k^2 p)$.

Due to its discontinuous nature, the enrichment may be removed by static condensation, resulting in a modified polynomial-Lagrange multiplier formulation [60], eliminating the zero diagonal block typically associated with the constraints. The enrichment is obtained as a postprocess within each element. This procedure, which ultimately simplifies and conditions the global formulation, should be done carefully, due to potential local ill-conditioning.

Element-level basis functions for u^{E} that satisfy Eq. (48) for constant k are plane waves of the form (24). Conditioning considerations may be used to determine the form of the plane wave [65]. The integration required to evaluate DEM matrices may be performed analytically for elements with flat faces and straight edges [66, 67].

A DEM element is a combination of enrichment and Lagrange multiplier configurations (with underlying low-order polynomials). Quadrilateral DEM elements are labeled "Quad-n_E-n_λ" where n_E is the number of plane wave enrichment functions in each element and n_λ is the number of Lagrange multipliers per edge (Fig. 13). Various DEM quadrilaterals are available: Quad-4-1 [60], Quad-8-2 [68], Quad-12-3 [65], Quad-16-4, and Quad-32-8 [69].

Full approximation of the Lagrange multipliers as the normal derivative of the enrichment is often undesirable due to stability considerations of the hybrid numerical method. A necessary algebraic condition to ensure a nonsingular global coefficient matrix [68] is

$$n_{eb} n_\lambda \leq 2 n_E$$

for n_{eb} element boundaries. The ratio of four between the number of plane waves in the enrichment and the number of Lagrange multipliers per edge of the quadrilaterals conforms to this algebraic condition. The basis functions for the approximate Lagrange multipliers are *modified* plane waves, restricted to the edges, designed to improve the dispersion performance [65], see Section 5.2. Conditioning considerations may be used to determine the form of the plane wave [65].

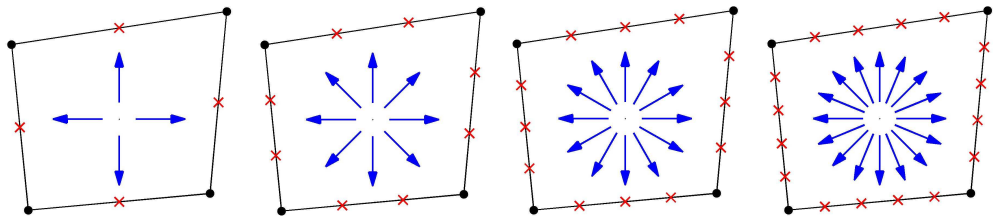

FIGURE 13. Quadrilateral DEM elements, from left to right: Quad-4-1, Quad-8-2, Quad-12-3, and Quad-16-4

5.2 Dispersion Analysis

As in continuous formulations, dispersion analysis is performed for the free-space, homogeneous, constant-coefficient Helmholtz equation, for which plane waves are exact solutions, on translation invariant meshes [70]. The analysis is applied to the statically condensed form of the DEM equations, focusing on the Lagrange multipliers. Due to the local support of the Lagrange multipliers, defined on element boundaries, each stencil couples only the degrees of freedom of the two adjacent elements sharing a boundary. The analysis leads to a set of homogeneous linear algebraic equations for unknown amplitudes, with coefficients that depend on the unknown approximate wave number of the constraint field k^C. Nontrivial solutions exist when the coefficient matrix is singular. Thus the dispersion relation between between the numerical and exact wave numbers is the characteristic equation, which is usually evaluated numerically.

The Quad-4-1 element is enriched with four plane waves in the positive and negative axis directions. The Lagrange multipliers are constants on the element edges. The dispersion analysis is based on two repeating stencils, related to Lagrange multipliers approximating normal derivatives along both axes, resulting in a system of two homogeneous equations. The dependence of the dispersion in the constraint field of the Quad-4-1 element on resolution G and orientation of the mesh with respect to the direction of propagation θ^* is shown in Fig. 14.

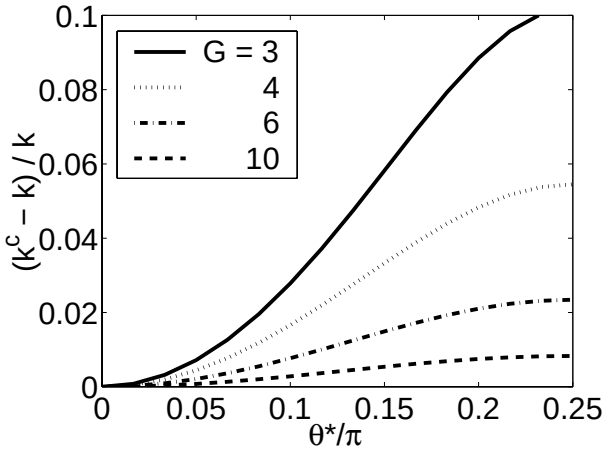

FIGURE 14. Dispersion in the constraint field of the Q-4-1 element at various resolutions, $G = 2\pi/(kh)$

The dispersion analysis of a quadrilateral DEM element with n_λ Lagrange multipliers per edge results in a system of $2n_\lambda$ homogeneous equations. The modified wave number in the Lagrange multiplier plane-wave basis functions is selected to minimize the maximum dispersion [65].

5.3 Tetrahedral Element

Hexahedral DEM elements are available for a few years [71]. The generation of uniform spherical directions is more involved than in the plane. One approach is to choose the directions from the element center to face nodes of Lagrange elements of cubic geometry ([71], Algorithm 1), with special node positioning to improve uniformity. Alternatively, one can minimize the maximum distance of any point on a sphere from the closest point [72]. A correction of Beverly's triangulation technique from the field of crystallography for finding equally-spaced points on latitudinal lines of a sphere [67] is another option. This notion leads to competitive hexahedral elements (Fig. 15).

There are many practical difficulties in the generation of hexahedral meshes so that tetrahedral elements are often used in three-dimensional problems. Triangular elements provide a prelude to the development of tetrahedral elements [65]. Of the different configurations considered, those with equally spaced enrichment, which is invariant to the element geometry, identical to the corresponding quadrilaterals (Fig. 16), perform the best. The dispersion analysis in this case is performed on a hexagonal mesh of equilateral triangles.

Of the tetrahedral elements examined, those based on the corrected Beverly technique (Fig. 17), show the best performance [67]. Regular tetrahedra would be desirable for dispersion analysis, but they are not space fillers. Instead, 48 trirectangular tetrahedra are used to form a rhombic dodecahedron pattern, which is a space filler. Thus the dispersion relation is the characteristic equation of a system of $48n_\lambda$ homogeneous equations.

The tetrahedral DEM elements are compared numerically to the standard linear, quadratic, and cubic tetrahedral elements, labeled "Tet1," "Tet2," and "Tet3," respectively, to assess efficiency. Consider a wave guide problem in a cube of side L. Robin boundary conditions are specified so that the exact solution is a plane wave propagating in a given di-

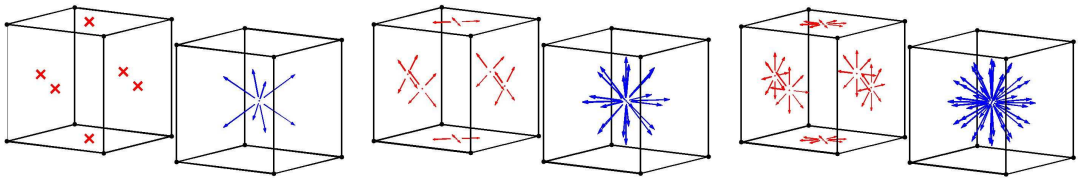

FIGURE 15. Hexahedral DEM elements: Hex-8-1 (left), Hex-22-4 (center), and Hex-46-8

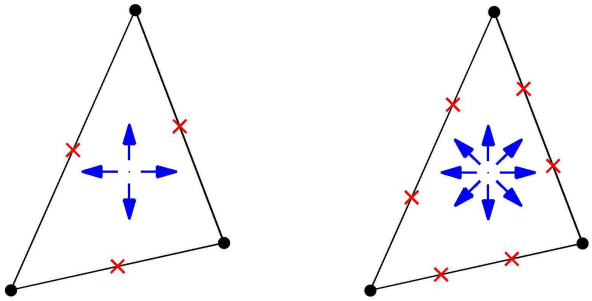

FIGURE 16. Triangular DEM elements: Tri-4-1 (left) and Tri-8-2

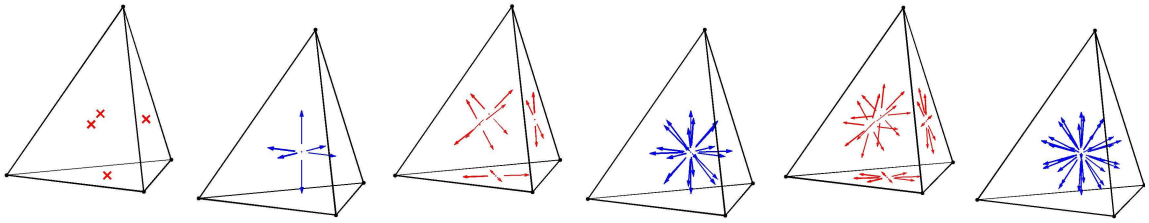

FIGURE 17. Tetrahedral DEM elements: Tet-6-1 (left), Tet-22-4 (center), and Tet-34-8

rection. Nondimensional wave numbers, $kL = 4$ and 8, are examined. The domain is discretized by a sequence of uniform cubical divisions of size h, from 1 to $8 \times 8 \times 8$. Each cube is divided into six tetrahedra (Fig. 18). Resolutions vary from fewer than 2 elements per wavelength ($kL = 8$) to more than 15 ($kL = 4$).

Results for a plane wave propagating at a longitude (or azimuth) and colatitude (or polar) angle $\theta = \phi = 50°$, in a k-scaled modified H^1 seminorm (squared) $|\bar{u}^h - u|^2_{H^1(\tilde{\Omega})} + k\|[\![\bar{u}^h]\!]\|^2_{L_2(\tilde{\Gamma}\setminus\Gamma)}$, are reported in Fig. 19. Little pollution is observed in the results of the Tet-22-4 and Tet-34-8 elements (the error is almost independent of kL). Approximate rates of convergence are presented. The proposed configurations of tetrahedral DEM elements become more

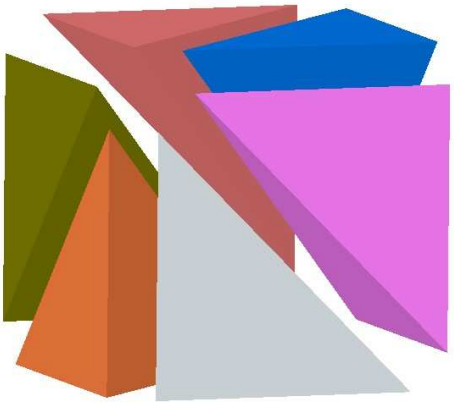

FIGURE 18. Cube division into six tetrahedra

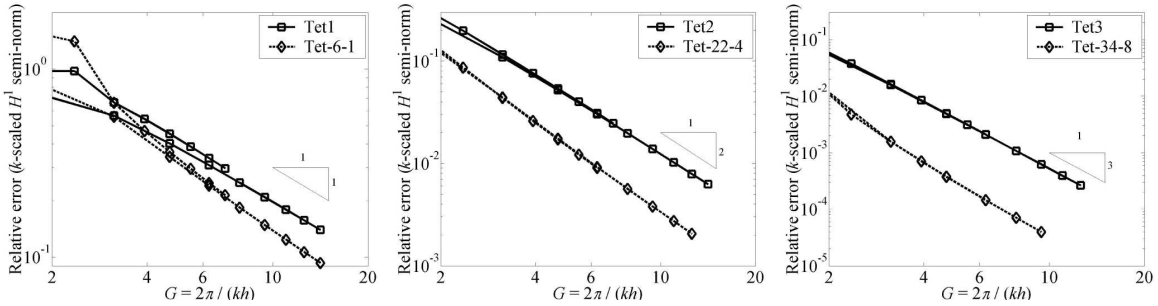

FIGURE 19. Relative error of tetrahedral DEM elements ($kL = 4$ and 8, $\theta = \phi = 50°$)

competitive as the enrichment and Lagrange multipliers are enhanced.

6. SUMMARY

The development of efficient discretization schemes for acoustics is a challenge due to the numerical difficulties that arise in the solution of wave problems, particularly at high wave numbers. Since computation naturally separates the scales of a problem according to the mesh size, multiscale considerations provide a useful framework for viewing these difficulties and developing methods to counter them. Tremendous progress has been made in recent years. The diversity of these contributions demonstrates both the breadth of the numerical methodology which is now applied to acoustic problems and the many possibilities that exist for future research in this area.

REFERENCES

1. Zienkiewicz, O. C., Achievements and Some Unsolved Problems of the Finite Element Method. *Int. J. Numer. Methods Eng.* **47**:9–28, 2000.
2. Babuška, I., Ihlenburg, F., Paik, E. T., and Sauter, S. A., A Generalized Finite Element Method for Solving the Helmholtz Equation in Two Dimensions with Minimal Pollution. *Comput. Methods Appl. Mech. Eng.* **128**:325–359, 1995.
3. Ihlenburg, F., *Finite Element Analysis of Acoustic Scattering*. Springer, New York, 1998.
4. Chertock, G., Integral Equation Methods in Sound Radiation and Scattering from Arbitrary Structures. *NSRDC Technical Report 3538*, David W. Taylor Naval Ship Research and Development Center, Bethesda, MD, 1971.
5. Kleinman, R. E., and Roach, G. F., Boundary Integral Equations for the Three-Dimensional Helmholtz Equation. *SIAM Rev.* **16**:214–236, 1974.
6. Shaw, R. P., Integral Equation Methods in Acoustics. In *Boundary Elements X*, Brebbia, C. A., Ed. Computational Mechanics Publications, Southampton, **4**:221–244, 1988.
7. Burnett, D. S., A Three-Dimensional Acoustic Infinite Element Based on a Prolate Spheroidal Multipole Expansion. *J. Acoust. Soc. Am.* **96**:2798–2816, 1994.
8. Harari, I., and Hughes, T. J. R., A Cost Comparison of Boundary Element and Finite Element Methods for Problems of Time-Harmonic Acoustics. *Comput. Methods Appl. Mech. Eng.* **97**:77–102, 1992.
9. Chen, J.-T., and Chen, K.-H., Applications of the Dual Integral Formulation in Conjunction with Fast Multipole Method in Large-Scale Problems for 2D Exterior Acoustics. *Eng. Anal. Bound. Elem.* **28**:685–709, 2004.
10. Greengard, L., Huang, J., Rokhlin, V., and Stephen, W., Accelerating Fast Multipole Methods for the Helmholtz Equation at Low Frequencies. *IEEE Comput. Sci. Eng.* **5**:32–38, 1998.
11. Franca, L. P., and Dutra do Carmo, E. G., The Galerkin Gradient Least-Squares Method. *Comput. Methods Appl. Mech. Eng.* **74**:41–54, 1989.
12. Harari, I., and Hughes, T. J. R., Galerkin/Least-Squares Finite Element Methods for the Re-

duced Wave Equation with Nonreflecting Boundary Conditions in Unbounded Domains. *Comput. Methods Appl. Mech. Eng.* **98**:411–454, 1992.

13. Givoli, D., Non-Local and Semi-Local Optimal Weighting Functions for Symmetric Problems Involving a Small Parameter. *Int. J. Numer. Methods Eng.* **26**:1281–1298, 1988.
14. Demkowicz, L., and Oden, J. T., An Adaptive Characteristic Petrov-Galerkin Finite Element Method for Convection-Dominated Linear and Nonlinear Parabolic Problems in Two Space Variables. *Comput. Methods Appl. Mech. Eng.* **55**:63–87, 1986.
15. Barbone, P. E., and Harari, I., Nearly H^1-Optimal Finite Element Methods. *Comput. Methods Appl. Mech. Eng.* **190**:5679–5690, 2001.
16. Hughes, T. J. R., Multiscale Phenomena: Green's Functions, the Dirichlet-to-Neumann Formulation, Subgrid Scale Models, Bubbles and the Origins of Stabilized Methods. *Comput. Methods Appl. Mech. Eng.* **127**:387–401, 1995.
17. Hughes, T. J. R., Feijóo, G. R., Mazzei, L., and Quincy, J.-B., The Variational Multiscale Method - A Paradigm for Computational Mechanics. *Comput. Methods Appl. Mech. Eng.* **166**:3–24, 1998.
18. Franca, L. P., and Farhat, C., Bubble Functions Prompt Unusual Stabilized Finite Element Methods. *Comput. Methods Appl. Mech. Eng.* **123**:299–308, 1995.
19. Brezzi, F., Bristeau, M. O., Franca, L. P., Mallet, M., and Rogé, G., A Relationship between Stabilized Finite Element Methods and the Galerkin Method with Bubble Functions. *Comput. Methods Appl. Mech. Eng.* **96**:117–129, 1992.
20. Brezzi, F., and Russo, A., Choosing Bubbles for Advection-Diffusion Problems. *Math. Models Methods Appl. Sci.* **4**:571–587, 1994.
21. Brezzi, F., Franca, L. P., and Russo, A., Further Considerations on Residual-Free Bubbles for Advective-Diffusive Equations. *Comput. Methods Appl. Mech. Eng.* **166**:25–33, 1998.
22. Franca, L. P., Farhat, C., Macedo, A. P., and Lesoinne, M., Residual-Free Bubbles for the Helmholtz Equation. *Int. J. Numer. Methods Eng.* **40**:4003–4009, 1997.
23. Franca, L. P., Nesliturk, A., and Stynes, M., On the Stability of Residual-Free Bubbles for Convection-Diffusion Problems and Their Approximation by a Two-Level Finite Element method. *Comput. Methods Appl. Mech. Eng.* **166**:35–49, 1998.
24. Brezzi, F., Franca, L. P., Hughes, T. J. R., and Russo, A., $b = \int g$. *Comput. Methods Appl. Mech. Eng.* **145**:329–339, 1997.
25. Franca, L. P., Madureira, A. L., and Valentin, F., Towards Multiscale Functions: Enriching Finite Element Spaces with Local but Not Bubble-Like Functions. *Comput. Methods Appl. Mech. Eng.* **1940**:3006–3021, 2005.
26. Hou, T. Y., and Wu, X.-H., A Multiscale Finite Element Method for Elliptic Problems in Composite Materials and Porous Media. *J. Comput. Phys.* **134**:169–189, 1997.
27. Hughes, T. J. R., and Sangalli, G., Variational Multiscale Analysis: The Fine-Scale Green's Function, Projection, Optimization, Localization, and Stabilized Methods. *SIAM J. Numer. Anal.* **45**:539–557, 2007.
28. Franca, L. P., Frey, S. L., and Hughes, T. J. R., Stabilized Finite Element Methods. I. Application to the Advective-Diffusive Model. *Comput. Methods Appl. Mech. Eng.* **95**:253–276, 1992.
29. Franca, L. P., and Valentin, F., On an Improved Unusual Stabilized Finite Element Method for the Advective-Reactive-Diffusive Equation. *Comput. Methods Appl. Mech. Eng.* **189**:1785–1800, 2000.
30. Harari, I., and Magoulès, F., Numerical Investigations of Stabilized Finite Element Computations for Acoustics. *Wave Motion*. **39**:339–349, 2004.
31. Thompson, L. L., and Pinsky, P. M., A Galerkin Least-Squares Finite Element Method for the Two-Dimensional Helmholtz Equation. *Int. J. Numer. Methods Eng.* **38**:371–397, 1995.
32. Stewart, J. R., and Hughes, T. J. R., h-Adaptive Finite Element Computation of Time-Harmonic Exterior Acoustics Problems in Two Dimensions. *Comput. Methods Appl. Mech. Eng.* **146**:65–89, 1997.
33. Kechroud, R., Soulaimani, A., Saad, Y., and Gowda, S., Preconditioning Techniques for the

Solution of the Helmholtz Equation by the Finite Element Method. *Math. Comput. Simul.* **65**:303–321, 2004.

34. Oberai, A. A., and Pinsky, P. M., A Residual-Based Finite Element Method for the Helmholtz Equation. *Int. J. Numer. Methods Eng.* **49**:399–419, 2000.
35. Harari, I., and Hughes, T. J. R., Finite Element Methods for the Helmholtz Equation in an Exterior Domain: Model Problems. *Comput. Methods Appl. Mech. Eng.* **87**:59–96, 1991.
36. Harari, I., Finite Element Dispersion of Cylindrical and Spherical Acoustic Waves. *Comput. Methods Appl. Mech. Eng.* **190**:2533–2542, 2001.
37. Cherukuri, H. P., Dispersion Analysis of Numerical Approximations to Plane Wave Motions in an Isotropic Elastic Solid. *Comput. Mech.* **25**:317–328, 2000.
38. Christon, M. A., The Influence of the Mass Matrix on the Dispersive Nature of the Semi-Discrete, Second-Order Wave Equation. *Comput. Methods Appl. Mech. Eng.* **173**:147–166, 1999.
39. Christon, M. A., and Voth, T. E., Results of von Neumann Analyses for Reproducing Kernel Semi-Discretizations. *Int. J. Numer. Methods Eng.* **47**:1285–1301, 2000.
40. Deraemaeker, A., Babuška, I., and Bouillard, P., Dispersion and Pollution of the FEM Solution for the Helmholtz Equation in One, Two and Three Dimensions. *Int. J. Numer. Methods Eng.* **46**:471–499, 1999.
41. Harari, I., Reducing Spurious Dispersion, Anisotropy and Reflection in Finite Element Analysis of Time-Harmonic Acoustics. *Comput. Methods Appl. Mech. Eng.* **140**:39–58, 1997.
42. Krenk, S., Optimal Formulation of Simple Finite Elements. In *Variat. Methods Eng.* Springer, Berlin, 9.3–9.16, 1985.
43. Mullen, R., and Belytschko, T., Dispersion Analysis of Finite Element Semidiscretizations of the Two-Dimensional Wave Equation. *Int. J. Numer. Methods Eng.* **18**:11–29, 1982.
44. Oberai, A. A., and Pinsky, P. M., A Numerical Comparison of Finite Element Methods for the Helmholtz Equation. *J. Comput. Acoust.* **8**:211–221, 2000.
45. Harari, I., and Nogueira, C. L., Reducing Dispersion of Linear Triangular Elements for the Helmholtz Equation. *J. Eng. Mech.* **128**:351–358, 2002.
46. Lacroix, V., Bouillard, P., and Villon, P., An Iterative Defect-Correction Type Meshless Method for Acoustics. *Int. J. Numer. Methods Eng.* **57**:2131–2146, 2003.
47. Magoulès, F., Meerbergen, K., and Coyette, J.-P., Application of a Domain Decomposition Method with Lagrange Multipliers to Acoustic Problems Arising from the Automotive Industry. *J. Comput. Acoust.* **8**:503–521, 2000.
48. Harari, I., and Gosteev, K., Bubble-Based Stabilization for the Helmholtz Equation. *Int. J. Numer. Methods Eng.* **70**:1241–1260, 2007.
49. Strouboulis, T., Babuška, I., and Copps, K., The Design and Analysis of the Generalized Finite Element Method. *Comput. Methods Appl. Mech. Eng.* **181**:43–69, 2000.
50. Melenk, J. M., and Babuška, I., The Partition of Unity Method Finite Element Method: Basic Theory and Applications. *Comput. Methods Appl. Mech. Eng.* **139**:289–314, 1996.
51. Laghrouche, O., and Bettess, P., Short Wave Modelling Using Special Finite Elements. *J. Comput. Acoust.* **8**:189–210, 2000.
52. Goldstein, C. I., The Weak Element Method Applied to Helmholtz Type Equations. *Appl. Numer. Math.* **2**:409–426, 1986.
53. Cessenat, O., and Despres, B., Application of an Ultra Weak Variational Formulation of Elliptic PDEs to the Two-Dimensional Helmholtz Problem. *SIAM J. Numer. Anal.* **35**:255–299, 1998.
54. Monk, P., and Wang, D.-Q., A Least-Squares Method for the Helmholtz Equation. *Comput. Methods Appl. Mech. Eng.* **175**:121–136, 1999.
55. Ladevèze, P., Arnaud, L., Rouch, P., and Blanzé, C., The Variational Theory of Complex Rays for the Calculation of Medium-Frequency Vibrations. *Eng. Comput.* **18**:193–214, 2001.
56. Stojek, M., Least-Squares Trefftz-Type Elements for the Helmholtz Equation. *Int. J. Numer. Methods Eng.* **41**:831–849, 1998.
57. Cessenat, O., and Després, B., Using Plane Waves as Base Functions for Solving Time Harmonic Equations with the Ultra Weak Varia-

tional Formulation. *J. Comput. Acoust.* **11**:227–238, 2003.

58. van Hal, B., Desmet, W., Vandepitte, D., and Sas, P., A Coupled Finite Element-Wave Based Approach for the Steady-State Dynamic Analysis of Acoustic Systems. *J. Comput. Acoust.* **11**:285–303, 2003.
59. Alvarez, G. B., Loula, A. F. D., Dutra do Carmo, E. G., and Rochinha, F. A., A Discontinuous Finite Element Formulation for Helmholtz Equation. *Comput. Methods Appl. Mech. Eng.* **195**:4018–4035, 2006.
60. Farhat, C., Harari, I., and Franca, L. P., The Discontinuous Enrichment Method. *Comput. Methods Appl. Mech. Eng.* **190**:6455–6479, 2001.
61. Farhat, C., Harari, I., and Hetmaniuk, U., The Discontinuous Enrichment Method for Multiscale Analysis. *Comput. Methods Appl. Mech. Eng.* **192**:3195–3209, 2003.
62. Zhang, L., Tezaur, R., and Farhat, C., The Discontinuous Enrichment Method for Elastic Wave Propagation in the Medium-Frequency Regime. *Int. J. Numer. Methods Eng.* **66**:2086–2114, 2006.
63. Massimi, P., Tezaur, R., and Farhat, C., A Discontinuous Enrichment Method for Three-Dimensional Multiscale Harmonic Wave Propagation Problems in Multi-Fluid and Fluid-Solid Media. *Int. J. Numer. Methods Eng.* **76**:400–425, 2008.
64. Tezaur, R., Zhang, L., and Farhat, C., A Discontinuous Enrichment Method for Capturing Evanescent Waves in Multiscale Fluid and Fluid/Solid Problems. *Comput. Methods Appl. Mech. Eng.* **197**:1680–1698, 2008.
65. Grosu, E., and Harari, I., Studies of the discontinuous enrichment method for two-dimensional acoustics. *Finite Elem. Anal. Des.* **44**:272–287, 2008.
66. Gabard, G., Exact Integration of Polynomial-Exponential Products with Application to Wave-Based Numerical Methods. *Commun. Numer. Methods Eng.* doi:10.1002/cnm.1123, 2009.
67. Grosu, E., and Harari, I., Three-dimensional Element Configurations for the Discontinuous Enrichment Method for Acoustics. *Int. J. Numer. Methods Eng.* doi:10.1002/nme.2525, 2009.
68. Farhat, C., Harari, I., and Hetmaniuk, U., A Discontinuous Galerkin Method with Lagrange Multipliers for the Solution of Helmholtz Problems in the Mid-Frequency Regime. *Comput. Methods Appl. Mech. Eng.* **192**:1389–1419, 2003.
69. Farhat, C., Tezaur, R., and Weidemann-Goiran, P., Higher-Order Extensions of a Discontinuous Galerkin Method for Mid-Frequency Helmholtz Problems. *Int. J. Numer. Methods Eng.* **61**:1938–1956, 2004.
70. Harari, I., Tezaur, R., and Farhat, C., A Study of Higher-Order Discontinuous Galerkin and Quadratic Least-Squares Stabilized Finite Element Computations for Acoustics. *J. Comput. Acoust.* **14**:1–19, 2006.
71. Tezaur, R., and Farhat, C., Three-Dimensional Discontinuous Galerkin Elements with Plane Waves and Lagrange Multipliers for the Solution of Mid-Frequency Helmholtz Problems. *Int. J. Numer. Methods Eng.* **66**:796–815, 2006.
72. Huttunen, T., Seppälä, E. T., Kirkeby, O., Kärkkäinen, A., and Kärkkäinen, L., Simulation of the Transfer Function for a Head-and-Torso Model over the Entire Audible Frequency Range. *J. Comput. Acoust.* **15**:429–448, 2008.